Eur. Phys. J. A **3**, 139–147 (1998)

THE EUROPEAN PHYSICAL JOURNAL A

Superheavy nuclei in deformed mean–field calculations

T. Bürvenich[1], K. Rutz[1,2], M. Bender[1,3], P.–G. Reinhard[3,4], J. A. Maruhn[1,4], W. Greiner[1,4]

[1] Institut für Theoretische Physik, Universität Frankfurt, Robert–Mayer–Str. 10, D–60325 Frankfurt am Main, Germany
[2] Gesellschaft für Schwerionenforschung mbH, Planckstr. 1, D–64291 Darmstadt, Germany
[3] Institut für Theoretische Physik II, Universität Erlangen–Nürnberg, Staudtstr. 7, D–91058 Erlangen, Germany
[4] Joint Institute for Heavy–Ion Research, Oak Ridge National Laboratory, P. O. Box 2008, Oak Ridge, TN 37831, U.S.A

Received: 6 April 1998 / Revised version: 16 June 1998
Communicated by F. Lenz

Abstract. The ground–state properties of superheavy nuclei are investigated within various parametrisations of relativistic and nonrelativistic nuclear mean–field models. The heaviest known even–even nuclei starting with $Z=98$ are used as a benchmark to estimate the predictive power of the models and forces. From that starting point, deformed doubly magic nuclei are searched in the region $100\leq Z\leq 130$ and $142\leq N\leq 190$.

PACS. 21.30.Fe Forces in hadronic systems and effective interactions – 21.60.Jz Hartree-Fock and random-phase approximations – 24.10.Jv Relativistic models – 27.90.+b $220\leq A$

1 Introduction

The possible existence of shell–stabilized superheavy nuclei has been a strong motivation for heavy–ion physics since almost three decades [1–3]. Early theoretical estimates on the basis of the macroscopic–microscopic approach predicted the spherical doubly magic superheavy nucleus $^{298}_{184}114$ [2,3] which was a far away goal at that time. Much more elaborate macroscopic–microscopic calculations figured out an island of deformed shell closures around $Z=108$ [4,5]. This region has been accessed in recent experiments at GSI [6,7] and Dubna [8], where amongst many other isotopes the region around the expected *deformed* doubly magic nucleus $^{270}_{162}\mathrm{Hs}_{108}$ has been reached. The newly developed and the coming experimental facilities produce more and more new isotopes and the expected magic $Z=114$ seems to be in reach. Superheavy elements are thus a topic of current interest and it is worthwhile to look at it from various theoretical approaches. An alternative to the macroscopic–microscopic approach are the mean–field models which start from an effective energy–density functional and determine ground–state wave–functions and densities variationally in a self–consistent manner. The most widely used mean–field models in nuclear physics are the Skyrme–Hartree–Fock (SHF) approach (for a review see [9]), the Gogny force [10], and the relativistic mean–field model (RMF) (for reviews see [11–13]). We will consider here the SHF as well as the RMF to have one typical representative from the nonrelativistic and from the relativistic domain. Both models rely on a theoretically motivated and phenomenologically adjusted energy–density functional. The reliability of the actual parametrisations has developed very much since the first steps two and a half decades ago. With 6–10 free parameters, one obtains nowadays a very good reproduction of nuclear ground–state properties for the stable elements [12,14,15]. It is then very interesting to probe the descriptive power when extrapolating into the regime of the exotic nuclei which had not been accounted for in the adjustment of the forces. Investigations of light nuclei near the drip–lines have revealed that there are several loosely fixed aspects in these parametrisations (mainly isovector properties) [16]. The extrapolation towards superheavy nuclei challenges the predictive power in further respects (level structure, effective mass). There exist already several investigations of the shell structure of superheavy nuclei within self–consistent nuclear mean–field models [17–19], especially since there were early indications [20] that proton and neutron shell closures strongly affect each other and that $Z=120$ may be a shell closure rather than $Z=114$ as predicted by the macroscopic–microscopic models. In a recent systematic investigation of spherical superheavy nuclei covering about 15 different high–quality parametrisations within the SHF as well as the RMF, we have found very different predictions for shell closures, with even a $Z=126$ shell showing up as third alternative [17,21]. It is thus desirable to check the reliability of the models in the regime of the existing superheavy nuclei around $Z=108$ which requires, of course, deformed mean–field calculations. This is what we will present here. There is a further interesting aspect in these calculations. The macroscopic–microscopic method, although generally successful, requires preconceived knowledge about the expected shapes and single–particle potentials, which fades

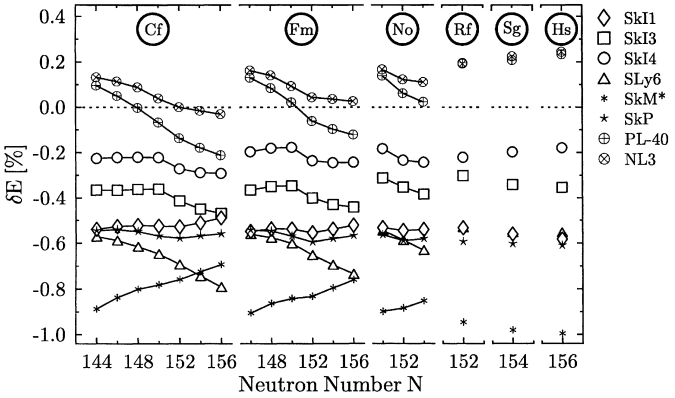

Fig. 1. Relative error of the binding energy in percent for the isotope chains of the heaviest known even–even nuclei, calculated with the forces as indicated. Negative values of δE correspond to under–bound nuclei, positive values to over–bound nuclei. The experimental data are taken from [30]

away when stepping into new regions. One has to remember that it took a long time to realize that higher order deformations are required to find the deformed shell closures [4,5]. Self–consistent calculations, on the other hand, provide deformed ground states in an unprejudiced manner within the chosen symmetry. They thus provide a valuable complement to the macroscopic–microscopic calculations.

The paper is outlined as follows: In Sec. 2 we explain briefly the models and parametrisations used. In Sec. 3 we present and discuss the results.

2 The framework

For both the SHF as well as the RMF there exists a widespread literature. Therefore we can skip a detailed presentation of the formalism and resulting self–consistent equations.

There remains the problem of choosing a parametrisation out of the overwhelming variety of published forces (more than 60 for SHF and about 20 for the RMF model). A decision was worked out in a previous study of spherical superheavy nuclei [21]. To that end, we had preselected 10 parametrisations for SHF and 5 for the RMF model which all represented an up–to–date quality of describing the ground–state properties for the existing stable nuclei. We confine this further to 6 parametrisations for SHF and two for RMF in order to keep the presentation just manageable. The selection of SHF forces is: SkM* as a widely used standard which also guarantees reasonable fission barriers [22]; SkP was developed around the same time as a force tuned for full nuclear HFB calculations [23] and here serves as a representative for effective mass $m^*/m = 1$ (all other forces have lower effective masses $0.55 \leq m^*/m \leq 0.8$); SLy6 is a recent fit which aims at describing extremely neutron–rich systems up to neutron stars [14]; SkI1–SkI4 stem from a recent investigation of spectral properties and isotopic shifts [15] where SkI1 is a fit within the old standard parametrisation, SkI3 is a similar fit with the isovector spin–orbit force in exact analogy to the RMF, and SkI4 a fit with additionally freely varied isovector spin–orbit force. This sample is typical for the wide span of choices within SHF and particularly contains a systematic variation of spectral properties (m^*/m and spin–orbit) crucial for the prediction of superheavy nuclei. There is less variance in the RMF parametrisations as the spin–orbit force and the effective mass is more or less fixed. There remains some choice in the isovector properties and we thus consider two forces: PL–40, a variant with stabilized meson self–coupling (we have checked that the results from PL–40 and the widely used standard nonlinear force NL–Z [12] do not differ visibly for the observables we will study in the following), as representative of fits biased on stable nuclei [24,12] and NL3 as a recent fit which tries to perform better with respect to exotic nuclei with large isotopic chains [25]. We will see later that even this narrow selection covers a large variance concerning the average quality of the binding energies in the known superheavy nuclei. Nevertheless we will restrict part of the discussions to a tight subselection of two forces, SkI4 for SHF and PL–40 for the RMF.

Table 1. Pairing strengths V_n for the neutrons and V_p for the protons for the mean–field forces used in this study. m^*/m is the isoscalar effective mass in infinite nuclear matter. Note that the absolute value of the pairing strength decreases with increasing effective mass

Force	m^*/m	V_n [MeV]	V_p [MeV]
SkM*	0.789	−276	−292
SkP	1.0	−241	−265
SkI1	0.693	−320	−305
SkI3	0.574	−340	−351
SkI4	0.650	−310	−324
SLy6	0.689	−308	−320
PL–40	0.581	−346	−348
NL3	0.595	−329	−342

In both SHF and RMF the pairing correlations are treated in the BCS scheme using a delta pairing force [26] $V_\mathrm{pair} = V_\mathrm{p/n}\,\delta(\boldsymbol{r}_1 - \boldsymbol{r}_2)$. The pairing strengths V_p for protons and V_n for neutrons depend on the actual mean–field parametrisation, see table 1. They are optimized by fitting for each parametrisation separately the pairing gaps from a fourth–order finite–difference formula of binding energies in isotopic and isotonic chains of semi–magic nuclei throughout the chart of nuclei. The pairing–active space is chosen to include the number of one additional shell of oscillator states above the Fermi energy with a smooth Fermi cutoff weight, for details see [27]. Furthermore, a center–of–mass correction is performed. The actual recipe depends on the parametrisation. For the SkIx forces, SLy6 and PL–40, we use the prescription to subtract a posteriori $E_\mathrm{c.m.} = \langle \hat{\mathbf{P}}^2_\mathrm{c.m.} \rangle / (2mA)$, see [12,28]. For NL3, the harmonic oscillator estimate $E_\mathrm{c.m.} = (3/4)\,41\,A^{-1/3}$ MeV is subtracted, while for SkM* and SkP only a diagonal correction is performed [28], as used in the original adjust-

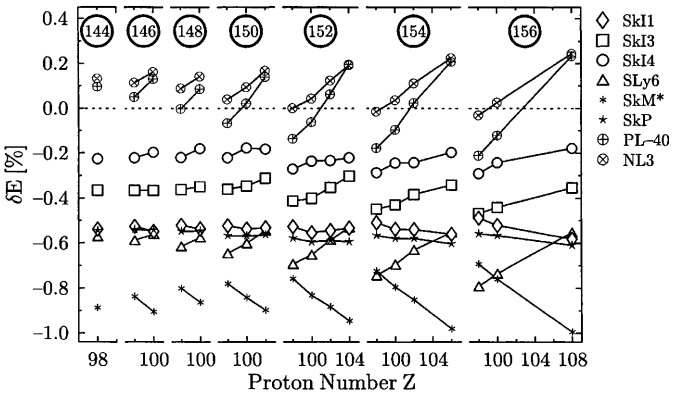

Fig. 2. The same as in Fig. 1, but for isotone chains with the neutron numbers as indicated

ment of these parameter sets. The numerical procedure represents the coupled SHF and RMF equations on a grid in coordinate space using a Fourier definition of the derivatives and solves them with the damped gradient iteration method [29]. We consider axially symmetric deformed states and thus use cylindrical coordinates for the numerical representation. Both models have been implemented in a common programming environment sharing all the crucial basic routines. We want to point out that we consider ground states throughout the paper. These ground states are determined self–consistently without any assumptions about the nuclear shapes.

3 Results and discussion

3.1 Comparison with experimental binding energies

The most important, and for most superheavy nuclei the only quantitatively known, global ground–state property is the binding energy. Figures 1 and 2 show the relative error of the binding energy

$$\delta E = \frac{E_{\rm calc} - E_{\rm expt}}{E_{\rm expt}} \qquad (1)$$

in percent for the heaviest known even–even nuclei, calculated in an axial representation with the mean–field parametrisations as indicated. The experimental values are taken from [30]. Negative values of δE correspond to under–bound nuclei, while for positive values the absolute value of the calculated binding energy is too large. The same results are drawn twice, once versus neutron number to display isotopic trends and once versus proton number for the isotonic trends. The first impression from the figures is that all forces come fairly close to the experimental results, usually with deviations below 1%. It is to be remembered that the average precision of these forces is about 0.3% precision for the conventional stable nuclei. One looses, of course, this level of accuracy when proceeding to extrapolations. But the remaining 1% demonstrate a still satisfying predictive power of the mean–field models in general. In this subsection we discuss the error of the absolute binding energy, and it should be kept in mind that there are some uncertainties in the calculated binding energy. There is an uncertainty due to the numerical solution of the equations of motion which is, however, safely below 0.1 MeV and thus negligible in our calculations. The prescription of pairing adds another uncertainty to the calculated binding energies. We use the same pairing scheme and force for all calculations with an optimized strength for each mean–field parametrisation. The use of a local pairing force improves the description of pairing correlations within the BCS scheme compared to a constant force or the constant gap approach [27], and removes some problems concerning the coupling of continuum states to the nucleus. From the possible variation of pairing recipes, we infer an uncertainty of the total binding energy of approximately 1 MeV, corresponding to an uncertainty of the relative errors of 0.05% [31]. The center–of–mass correction is also performed approximately, yielding only small uncertainties of approximately 0.2 MeV for these heavy systems [32]. In our calculations we neglect the correction for spurious rotational and vibrational modes, which can increase the binding energy up to 1 MeV [33], and is negligible for the present discussion.

At second glance, we see that the deviations are not distributed stochastically but show clear trends. First, there is a general offset for each force, and second, the deviations line up along one slope in isotopic or isotonic trends. The general offset comes as a consequence of a long–range trend with mass number. Comparing the different forces, we see large differences in the quality for this particular region of the nuclear chart, although all forces have comparable quality in the regime of stable nuclei. This is a typical behavior of an extrapolation. It is, however, gratifying that there remain enough forces which provide good quality also for these superheavy nuclei. The average relative error of the binding energies calculated with PL–40, NL3 and SkI4 stays within the 0.3% demanded for the fit nuclei. Although the results from the relativistic forces NL3 and PL–40 are somewhat closer to the experimental data than those obtained with the nonrelativistic SkI4, one has to take into account as an additional criterion the slopes of the errors of the binding energy, which hint at an unresolved isotopic or isotonic trend. Non–zero slopes correspond to an error in the separation energies. From the three preferred forces, SkI4 leads to the best (near zero) slopes whereas significant isotopic and isotonic trends remain in the RMF models.

For completeness, we ought to mention that binding energies of superheavy nuclei have been studied extensively in two approaches which are related to the present mean–field models, the finite–range droplet model (FRDM) [34] and extended Thomas–Fermi with Skyrme interactions (ETFSI) [35].The FRDM describes the global trends of binding energies $E_{\rm B}$ with a very elaborate liquid–drop model and adds the detailed fluctuations by the shell correction method using a standard parametrisation of the nuclear shell model. The free parameters of the FRDM are fitted to a huge pool of data on $E_{\rm B}$, and these fits yield

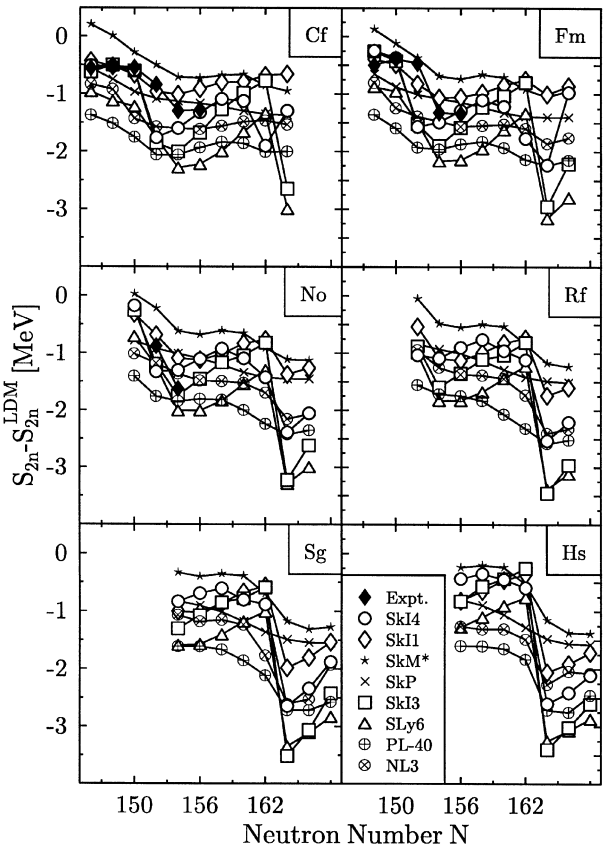

Fig. 3. Two–neutron separation energy S_{2n} for isotope chains of superheavy nuclei. To enlarge the shell effects, the smooth liquid–drop trend of the separation energies has been subtracted

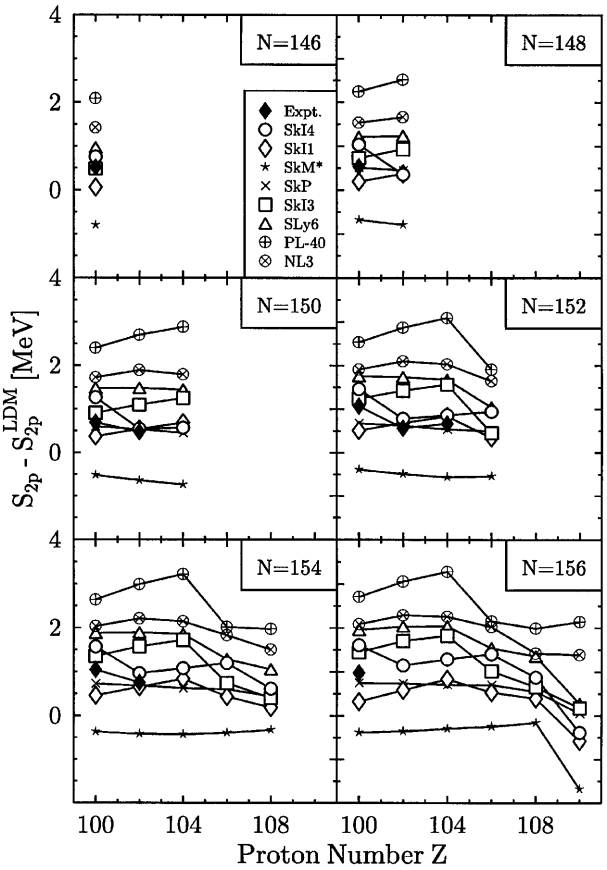

Fig. 4. The same as in Fig. 3, but for the two–proton separation energy S_{2p} in the isotone chains with the neutron number as indicated

a remarkable reproduction of the E_B with a typical error of $\Delta E_B = \pm 0.7$ MeV. The ETFSI lies between the FRDM and the mean–field models considered here. It is based on a SHF description, but solves the mean–field equations in a semi–classical approach (ETF) and adds shell corrections a posteriori, as in the FRDM, but here they are deduced self–consistently from the ETF mean–field. The parameters of the underlying SHF model, i.e., the force SkSC4, are fitted aiming at optimal description of binding energies. The resulting rms error is 0.74 MeV, quite similar to the FRDM. The FRDM and ETFSI, being concerned exclusively with E_B, thus differ in their descriptive bias from the other mean–field models which aim at a much broader range of observables, considering radii, form–factors, giant resonances and possibly more. At least we can learn from these approaches with bias on energies that the limit of achievable precision of mean–field models is somewhere near 0.7 MeV. Moreover, the FRDM and ETFSI have already been extended to include data on superheavy nuclei (which is not the case for all the SHF and RMF parametrisations discussed here). It is found that the new data can be accommodated very well within the given rms error. This agrees with our findings deduced from Figs. 1 and 2, namely that there are indeed some parametrisations out of the manifold of existing forces which provide a good description for the known superheavy nuclei. The agreement could even be much improved when including these new data specifically in the adjustment, a step which has yet to come for SHF and RMF. The interesting open question is whether this statement extends further into the superheavy region where details of shell structure become even more crucial.

3.2 Two–nucleon separation energies

As we have seen, trends can serve as observables that are as important as the binding energy itself. The trends are directly related to the two–neutron and two–proton separation energies

$$S_{2n}(N,Z) = E(N-2,Z) - E(N,Z) \quad ,$$
$$S_{2p}(N,Z) = E(N,Z-2) - E(N,Z) \quad . \qquad (2)$$

For a better graphical discrimination, we scale away the smooth overall trend in the separation energies by subtracting from the experimental and calculated values the

corresponding separation energies calculated with the simple Bethe–Weizsäcker mass formula

$$E_{\rm LDM}(Z,A) = a_{\rm V}\,A + a_{\rm S}\,A^{2/3} + a_{\rm C}\,Z^2\,A^{-1/3} + a_{\rm A}\frac{(Z-A/2)^2}{A} \pm \delta \qquad (3)$$

and the parameters from [36].

Apart from shell closures, the experimental values of the resulting quantity $S_{2q} - S_{2q}^{\rm LDM}$ are approximately constant, while they show a sudden jump at a shell closure. Therefore it gives a more direct measure of shell closures than the two–nucleon separation energy itself. Figure 3 shows $S_{2q} - S_{2q}^{\rm LDM}$ for experimentally known two–neutron separation energies (full diamonds) in comparison with mean–field results for a variety of forces in the region of nuclei either known or accessible to experiment in the near future. The uncertainties of the binding energy as discussed in the last subsection cancel almost in this difference quantity.

The first impression is again that all forces perform fairly well staying within 1 MeV from the data. But the differences that have appeared in Figs. 1 and 2 also show up here if one looks for the details. We have seen already that the slope of PL–40 deviates from the slope of the experimental binding energies. This becomes apparent in Fig. 3 in that the results from PL–40 for the $S_{2\rm n}$ deviate from the data more than for several other forces. We see here a weakness of PL–40 concerning isotopic trends. The other RMF parametrisation, NL3, which was fitted with more emphasis on isotopic trends, performs better for the $S_{2\rm n}$. In any case, the SHF parametrisations generally come closer to the data. This is due to the fact that SHF has more isotopic flexibility than the RMF model and that thus isotopic trends can be better accommodated. The trends have been better adjusted in normal nuclei and this shines through even now in the extrapolation to the superheavy region.

Looking more closely at the trends of the $S_{2\rm n}$, we see a generally smooth pattern interrupted by occasional steps or kinks. Such a sudden step in the $S_{2\rm n}$ is a typical signature of a shell closure. The most pronounced steps are seen between $N=162$ and $N=164$ which is clearly related to the strong neutron shell closure at $N=162$ as seen in Fig. 5. The height of the step varies with Z and is largest at $Z=108$. It also varies with forces, being large for most SHF forces, smaller for the two relativistic cases, and absent for SkM* and SkP. A less pronounced step can be spotted between $N=150$ and $N=152$ for SkI3 and SkI4 indicating a weak shell closure at $N=150$. But the experimental data which are available for $Z=98$ and 100 do not show any signature of that step. They rather indicate a step at the next isotope $N=152$, particularly for $Z=100$. It is the force SLy6 which comes closest to this feature. We thus see that the very details of this region around $N=150$ are not perfectly reproduced by any one of the forces. One has to keep in mind that the step or shell closure there is only vaguely indicated in experiment as well as in the calculations. The region with a more pronounced shell closure is expected at $N=162$, and it is most interesting to see what future experimental data will show there.

Finally, in Fig. 4 we show results for the two–proton separation energies $S_{2\rm p}$ in comparison with the available experimental data. The most prominent difference to the previous figure is the more compressed energy scale which demonstrates that there are larger differences in the predictions of that observable. Again the SHF forces SkI1, SkI3 and SkI4 perform best overall. The more detailed analysis of steps (i.e. shell closures) is less conclusive here as the height of the steps is generally smaller than in case of the $S_{2\rm n}$. Nonetheless, we can spot in the longest chain (for $N=156$) a shell closure at $Z=108$ for most SHF models but at $Z=104$ for PL–40 and SkI3 (remember that the proton shell closure moves with increasing neutron number in case of SkI3, from $Z=104$ to $Z=108$, see Fig. 5). In any case, we see that the proton shell closures in that region of deformed superheavy nuclei are all rather weak. It will require a systematical investigation of a large set of data to pin down the effects.

3.3 Deformed shell closures

The search for magic shell closures in superheavy nuclei has accompanied the field from the beginning. A way to quantify magicity are the proton and neutron shell gaps

$$\delta_{2\rm n}(N,Z) = E(N+2,Z) - 2E(N,Z) + E(N-2,Z),$$
$$\delta_{2\rm p}(N,Z) = E(N,Z+2) - 2E(N,Z) + E(N,Z-2) \qquad (4)$$

which are taken in steps of two neutrons or protons, in order to avoid interference with the pairing gap. This quantity usually has small values for the majority of nuclei and develops sudden spikes at magic shell closures. The height of the peak quantifies how stable a shell closure is as compared to the neighboring background. As an example, the experimental values for the doubly magic ^{208}Pb are $\delta_{2\rm n} = 5.0\,$MeV and $\delta_{2\rm p} = 6.6\,$MeV. The shell gap decreases with increasing system size and gaps around 3 MeV can be considered as well developed shell closures in the realm of superheavy nuclei.

Figure 5 shows the shell gaps for all even–even nuclei in the considered region for a broad selection of SHF and RMF parametrisations. The dark horizontal stripes in the left panels (δ_{2p}) indicate the closed proton shells and the dark vertical stripes in the right panels the closed neutron shells (δ_{2n}). The grey scales are chosen such that larger values for the shell gaps are darker. Fully black squares indicate a value of the shell gap of about 3.5 MeV for protons and 2.5 MeV for neutrons. The different forces show quite different patterns for these shell gaps. This holds particularly for the proton shell closures. All SHF forces (SkM*, SkP, SLy6, SkI1, SkI3, SkI4) basically agree on predicting a closure at $Z=108$, however, with quite different amplitude of the gap. The RMF forces (NL3, PL–40) prefer smaller Z, 104 or 106. It is interesting that SkI3, the Skyrme parametrisation with an isospin dependence of the spin–orbit force similar to the RMF, shows shell

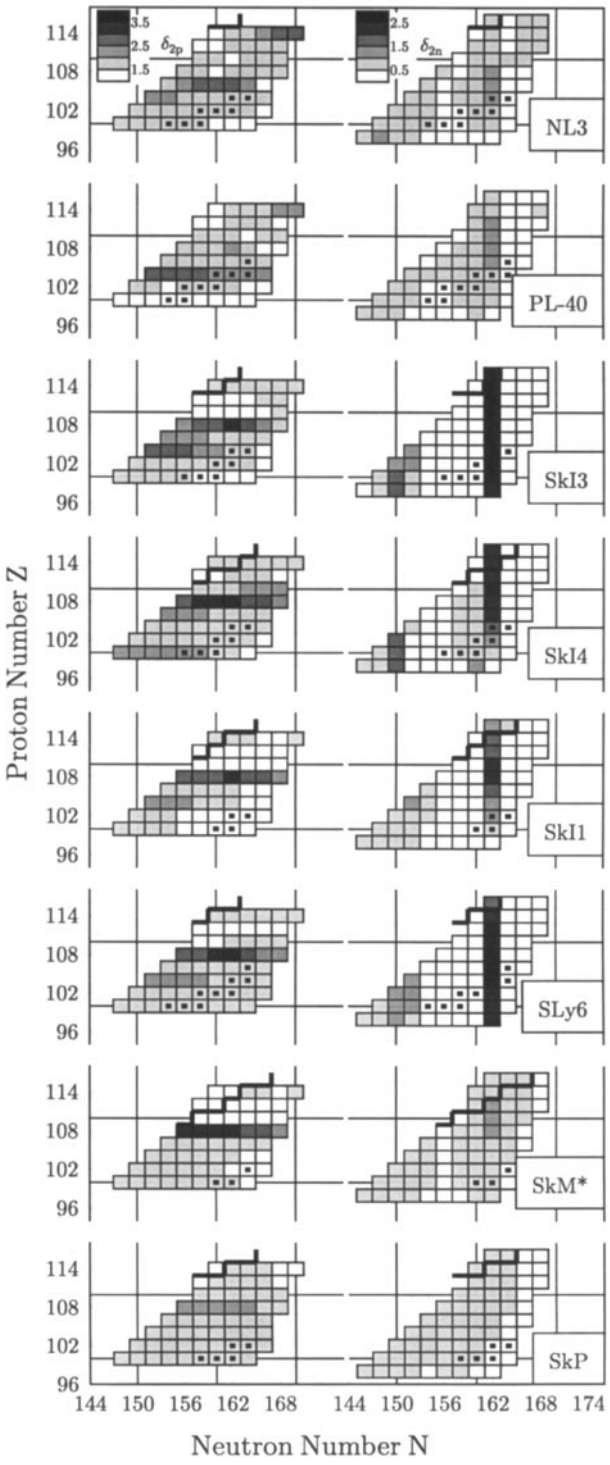

Fig. 5. Grey scale plots of proton shell gaps δ_{2p} (left column), and neutron shell gaps δ_{2n} (right column), in the N–Z plane as resulting from mean–field calculations in axial symmetry with the parametrisations as indicated. Note that scales of the shell gaps differ for protons and neutrons. The two–proton drip–line and β–stable nuclei are indicated by a heavy line and black squares, respectively

closures at $Z=104$ and at $Z=108$ as well. For the neutrons again the height of the shell gap varies substantially amongst the forces. But almost all forces agree in predicting a magic $N=162$. Some forces also show a hint of a shell closure at the smaller $N=150$, that does not appear in the experimental data as already discussed in Sec. 3.2. The shell closures are generally less pronounced for the Skyrme forces with large effective mass, i.e. SkM* and SkP, that therefore have the largest average level density in the vicinity of the Fermi energy of all the investigated parametrisations. The figure demonstrates the basic differences between SHF and RMF concerning proton shell closures and the more quantitative variation within each class of mean–field models. In order to look a bit more into detailed properties of the (deformed) shell closures in the considered mass range, we confine the next steps to two typical representatives, the force SkI4 for the SHF and PL–40 for the RMF model.

It was worked out already within the macroscopic–microscopic method that one will have deformed magic shell closures for $Z=108$ and $N=162$. This has only been found after carefully optimizing the ground states with deformations of higher multi–polarities in the shell model ansatz [4,5]. The mean–field models, on the other hand, deliver an arbitrarily deformed ground state at once as solution of the self–consistent equations. It is interesting to see which deformation properties emerge from the mean–field calculations. Figure 6 shows the two–proton and two–neutron shell gaps as well as the corresponding dimensionless quadrupole (β_2) and hexadecapole (β_4) moments

$$\beta_\ell = \frac{4\pi}{3AR^\ell}\langle r^\ell Y_{\ell 0}\rangle \quad \text{with} \quad R = 1.2\,A^{1/3}\ \text{fm} \qquad (5)$$

for SkI4 and PL–40 for a broader range of isotopes reaching up into the regime of the next spherical shell closures. The general features of the previous figure concerning shell closures persist. New is the information on deformation. A clear region of deformation is visible for the nuclides with small mass number $Z<110$, $N<170$, and equally clear is the restoration of spherical symmetry for the larger nuclei. There are slight differences between PL–40 and SkI4 concerning the upper end of the region of deformed ground states, that correspond to the different predictions for the next spherical magic proton number from these two forces [21]. It is to be noted that energetically competing oblate isomers exist for the heaviest systems in the sample with $N>184$.

The neutron shells are similar for SkI4 and PL–40. Both forces predict a spherical magic number $N=184$ and deformed shell closures at $N=162$ and 174. The spherical shell at $N=172$ in PL–40 appears only for proton numbers larger than $Z=120$ due to the onset of deformation going to smaller charge numbers.

There are clear differences concerning the proton shells. PL–40 predicts a deformed shell closure at $Z=104$ and a spherical shell closure at 120, whereas SkI4 offers a deformed $Z=108$ and various short stripes of spherical shell closures at $Z=114$, 120, 124, and, however, less pronounced at $Z=126$. The most interesting case is the occurrence of doubly magic nuclei, i.e., the coincidence of magic proton and neutron numbers. The predominant

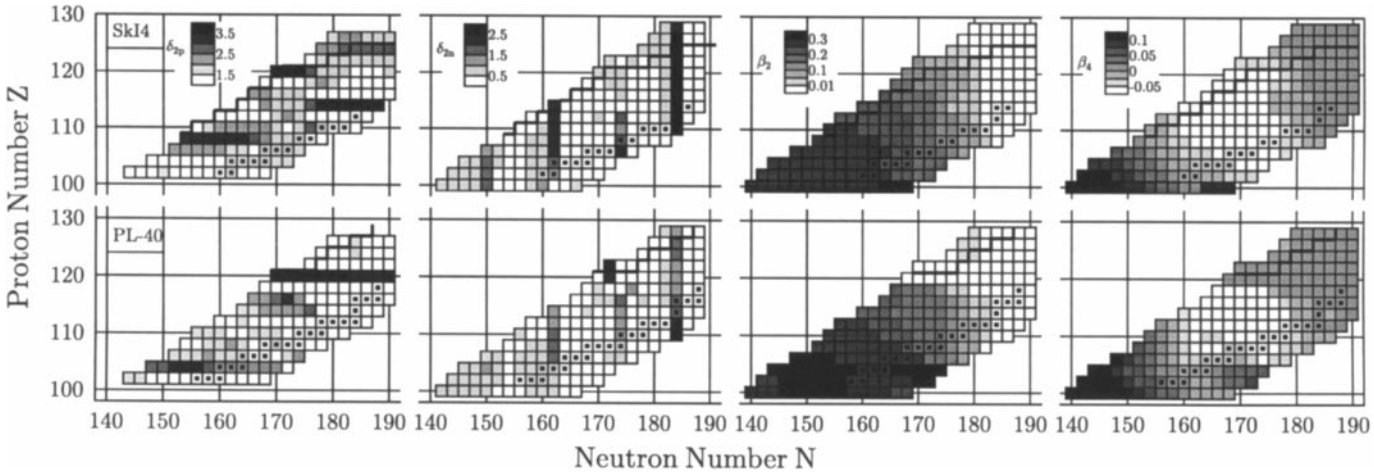

Fig. 6. Grey scale plots of proton shell gaps δ_{2p} (first column) neutron shell gaps δ_{2n}(right column), relative quadrupole moments β_2 (third column) and relative hexadecapole moments β_4 (right column) in the N–Z plane as they result from calculations in axial symmetry with the forces SkI4 (upper part) and PL–40 (lower part). The assignment of scales is indicated in the upper panels

one for PL–40 is the nucleus $^{292}_{172}120$, a secondary chance exists with $^{304}_{184}120$. Both are spherical, PL–40 predicts no deformed doubly magic nucleus in the superheavy region at all. Three doubly magic nuclei appear for SkI4, namely the deformed $^{270}_{162}108$ and the spherical $^{298}_{184}114$, $^{308}_{184}124$, and $^{310}_{184}126$. We see here again the same differences in the prediction of doubly magic nuclei as in our previous investigation of spherical superheavy nuclei [21]. One has to remember, however, that the shell gaps are anyway very small in these superheavy nuclei with their high level density, see Fig. 6. It remains yet to be seen to what extent such differences could have any practical consequences.

3.4 α–Decay half–lives

The lifetimes and decay channels of superheavy nuclei are of great importance for planned future experiments. The practical question is concerned with the stability of the superheavy elements. The shell gaps, studied above, provide one aspect which is related to the first fission barriers. Other important measures of stability are the α–decay Q–values and half–lives T_α, which are estimated here with the Viola systematics [37] using a recent fit of the parameters [38]. These two quantities, calculated from the binding energies computed with SkI4 and PL–40, are shown in Fig. 7. For both forces the nuclei in the valley of β–stability are rather stable. Consider, e.g., the $^{298}_{184}114$ nucleus: SkI4 predicts a half life of 10^{13} s and PL–40 gives 10^8 s. Going towards the proton–rich nuclei, one sees that PL–40 generally predicts more stable nuclei compared to SkI4. This is correlated with the two–proton drip–line which is closer to the valley of β–stability for SkI4 than for PL–40.

Drastic differences in the predictions of lifetimes occur for the nucleus $^{292}_{172}120$, which is doubly magic with PL–40 but not for SkI4. While for PL–40 there arises an area of increased stability with a life time of 10^4 s, SkI4 only predicts 10^{-4} s. This relates to the strong $Z=120$ and $N=172$ shells which do not occur for the parametrisation

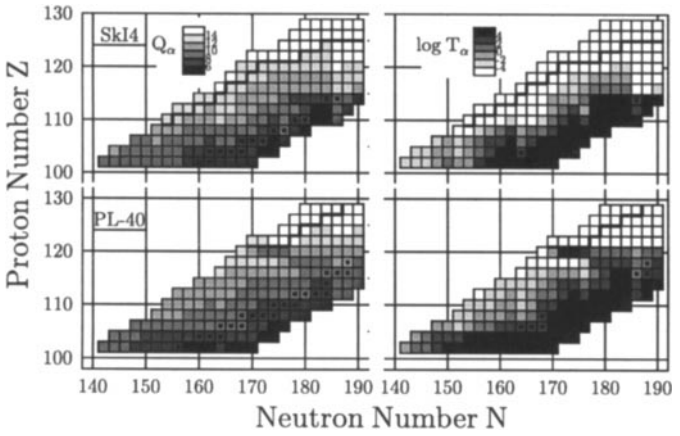

Fig. 7. Grey scale plots of Q_α values (left column) and the corresponding α–decay half lives estimated from Viola–Seaborg systematics (right column) as it results from SkI4 (upper part) and PL–40 (lower part). Scales are indicated in the upper boxes

SkI4. After all, one has to keep in mind that these α–decay half lives here are estimated by a semi–empirical formula and serve only as a guideline. The application of the Viola systematics requires that the landscape of fission barriers for the superheavy nuclei remains similar to the known heavy nuclei for which the systematics was developed. This needs yet to be checked.

4 Conclusions

We have investigated the capability of nuclear mean–field models to describe ground–state properties of superheavy nuclei. Two different approaches have been considered, the nonrelativistic Skyrme–Hartree–Fock scheme and the relativistic mean–field model. From the enormous manifold of available parametrisations for these two models, eight parametrisations have been selected for the present study,

two of them as "best candidates" with respect to overall quality together with good performance for superheavy elements, and five further choices as most typical variations. The study has covered elements in the range $100 \leq Z \leq 128$ and $140 \leq N \leq 190$ where experimental data are already available for the smaller samples.

The results of the mean–field models (in various parametrisations) have been compared with experimental data for the total binding energy. The binding energy as well as the two–neutron and two–proton separation energies are reproduced fairly well by all the considered parametrisations. A more detailed look reveals significant differences. Total binding energies are less well reproduced by those parametrisations which make compromises when fitting normal nuclei (e.g. sacrificing the surface tension which, in turn, deteriorates trends with mass number). Separation energies are more sensitive to the level structure and here we see a systematic difference between SHF and RMF, where SHF comes generally closer to the data. The mismatch of the RMF is due to its rigidity concerning isovector properties. There remains an open question at that point and it is most interesting to see a comparison for heavier systems where we expect more pronounced shell closures.

We have scanned the shell closures, deformations, and stability of all superheavy elements in the considered range. The SHF and the RMF deliver different predictions for doubly magic shell closures in regime of deformed closures as well as for spherical ones. Both models agree, however, in their predictions of deformations as such. The nuclei in the range $Z < 110$ and $N < 168$ have deformed ground states and the deformation extends to higher multi–polarities. These findings confirm the predictions of the macroscopic–microscopic models. The SHF and the RMF model differ in their estimates for proton shell closures. The RMF parametrisation PL–40 places them at $Z = 104$ (deformed) and 120 (spherical) whereas the SHF parametrisation SkI4 prefers $Z = 108$ (deformed), 114, and 124 (both spherical). Neutron shell closures are expected in both models at $N = 162$ (deformed) and 184 (spherical). PL–40 predicts additionally a spherical shell closure at $N = 172$. A faint shell closure is predicted at $N = 150$ from some mean–field models considered here whereas available experimental data on superheavy nuclei hint at a similarly faint shell closure for $N = 152$. But the relevance of this mismatch is not yet clear as this concerns small energy differences. The Q–values and half lives for α–decay show a difference between SHF and RMF when going towards proton–rich nuclei. The RMF model with PL–40 predicts more stability in that region.

The authors would like to thank S. Hofmann and G. Münzenberg for many valuable discussions. This work was supported by Bundesministerium für Bildung und Forschung BMBF, project no. 06 ER 808, by Deutsche Forschungsgemeinschaft (DFG), by Gesellschaft für Schwerionenforschung (GSI), and by Graduiertenkolleg Schwerionenphysik. The Joint Institute for Heavy Ion Research has as member institutions the University of Tennessee, Vanderbilt University, and the Oak Ridge National Laboratory; it is supported by the members and by the Department of Energy through Contract No. DE-FG05-87ER40361 with the University of Tennessee.

References

1. U. Mosel, B. Fink, W. Greiner, Contribution to *"Memorandum Hessischer Kernphysiker"* Darmstadt, Frankfurt, Marburg, 1966
2. U. Mosel, W. Greiner, Z. Phys. **217**, (1968) 256; Z. Phys. **222**, (1969) 261
3. S. G. Nilsson, C. F. Tsang, A. Sobiczewski, Z. Szymanski, S. Wycech, C. Gustafson, I.–L. Lamm, P. Möller, B. Nilsson, Nucl. Phys. **A131**, (1969) 1
4. Z. Patyk, A. Sobiczewski, Nucl. Phys. **A533**, (1991) 132
5. P. Möller, J. R. Nix, Nucl. Phys. **A549**, 84, (1992); J. Phys. **G20**, (1994) 1681
6. S. Hofmann, V. Ninov, F. P. Hessberger, P. Armbruster, H. Folger, G. Münzenberg, H. J. Schött, A. G. Popeko, A. V. Yeremin, A. N. Andreyev, S. Saro, R. Janik, M. Leino, Z. Phys. **A350**, (1995) 277 and Z. Phys. **A350**, (1995) 281
7. S. Hofmann, V. Ninov, F. P. Hessberger, P. Armbruster, H. Folger, G. Münzenberg, H. J. Schött, A. G. Popeko, A. V. Yeremin, S. Saro, R. Janik, M. Leino, Z. Phys. **A354**, (1996) 229
8. Yu. A. Lazarev, Yu. V. Lobanov, Yu. Ts. Oganessian, V. K. Utyonkov, F. Sh. Abdullin, A. N. Polyakov, J. Rigol, I. V. Shirokovsky, Yu. S. Tsyganov, S. Iliev, V. G. Subbotin, A. M. Sukhov, G. V. Buklanov, B. N. Gikal, V. B. Kutner, A. N. Mezentsev, K. Subotic, J. F. Wild, and R. W. Lougheed, K. J. Moody, Phys. Rev. C **54**, (1996) 620
9. P. Quentin, H. Flocard, Ann. Rev. Nucl. Part. Sci. **28**, (1978) 523
10. J. Dechargé, D. Gogny, Phys. Rev. **21**, (1980) 1568
11. B. D. Serot, J. D. Walecka, Adv. Nucl. Phys. **16**, (1986) 1
12. P.–G. Reinhard, Rep. Prog. Phys. **52**, (1989) 439
13. P. Ring, Prog. Part. Nucl. Phys. **37** (1996) 193
14. E. Chabanat, Ph. D. thesis, Lyon, 1996; E. Chabanat, P. Bonche, P. Haensel, J. Meyer, R. Schaeffer, preprint, 1996
15. P.–G. Reinhard, H. Flocard, Nucl. Phys. **A584**, (1995) 467
16. W. Nazarewicz, J. Dobaczewski, T. R. Werner, J. A. Maruhn, P.–G. Reinhard, K. Rutz, C. R. Chinn, A. S. Umar, M. R. Strayer, Phys. Rev. C **53**, (1996) 740
17. S. Ćwiok, J. Dobaczewski, P.-H. Heenen, P. Magierski, W. Nazarewicz, Nucl. Phys. **A611**, (1996) 211
18. J.–F. Berger, L. Bitaud, J. Dechargé, M. Girod, S. Peru–Dessenfants, Proceedings of the International Workshop XXXIV on Gross Properties of Nuclei and Nuclear Exitations, Hirschegg, Austria, January 1996. GSI, Darmstadt, 1996
19. G. A. Lalazissis, M. M. Sharma, P. Ring, Y. K. Gambhir, Nucl. Phys. **A608**, (1996) 202
20. M. Beiner, H. Flocard, M. Vénéroni, P. Quentin, Physica Scripta **10A**, (1974) 84
21. K. Rutz, M. Bender, T. Bürvenich, T. Schilling, P.–G. Reinhard, J. A. Maruhn, W. Greiner, Phys. Rev. C **56**, (1997) 238
22. J. Bartel, P. Quentin, M. Brack, C. Guet, H.–B. Håkansson, Nucl. Phys. **A386**, (1982) 79
23. J. Dobaczewski, H. Flocard, J. Treiner, Nucl. Phys. **A422**, (1984) 103

24. P.–G. Reinhard, Z. Phys. **A329**, (1988) 257
25. G. A. Lalazissis, J. König, P. Ring, Phys. Rev. C **55**, (1997) 540
26. S. J. Krieger, P. Bonche, H. .Flocard, P. Quentin, M. S. Weiss, Nucl. Phys. **A517**, (1990) 275
27. M. Bender, P.–G. Reinhard, K. Rutz, J. A. Maruhn, (in preparation)
28. J. Friedrich, P.–G. Reinhard, Phys. Rev. C **33**, (1986) 335
29. V. Blum, G. Lauritsch, J. A. Maruhn, P.–G. Reinhard, J. Comp. Phys. **100**, (1992) 364
30. G. Audi and A. H. Wapstra, Nucl. Phys. **A595**, (1995) 409
31. P.–G. Reinhard, W. Nazarewicz, M. Bender, J. A. Maruhn, Phys. Rev. C **53**, (1996) 2776
32. K. W. Schmid, P.–G. Reinhard, Z. Phys. **A530**, (1991) 283
33. P.–G. Reinhard, K. Goeke, Rep. Prog. Phys. **50**, (1987) 1
34. P. Möller, J. R. Nix, W. J. Swiatecki, At. Data Nucl. Data Tables **59**, (1995) 185
35. Y. Aboussir, J. M. Pearson, A. K. Dutta, F. Tondeur, At. Dat Nucl. Data Tables **61**, (1995) 127
36. A. H. Wapstra in: *Handbuch der Physik*, Band 38, Teil 1, *Springer Verlag*, Berlin–Göttingen–Heidelberg, 1958
37. V. E. Viola, Jr., G. T. Seaborg, J. Inorg. Nucl. Chem. **28**, (1966) 741
38. A. Sobiczewski, Z. Patyk und S. Cwiok, Phys. Lett. **224B**, (1989) 1